

$m_k = m_c \Delta N_c$, is a constant fraction, λ , of body mass: $m_k \approx \lambda m$. Thus $E_c dN_c/dt \approx E_c \Delta N_c/\Delta t \approx \lambda E_c m/m_c t_s$. The energy density of egg and other cells are similar, $E_e/m_e \approx E_c/m_c$, so this additional term becomes $E_c dN_c/dt \approx (\lambda E_c/t_s)N_c$. This is proportional to N_c and so has the identical structure to the maintenance term, $N_c B_c$, in equation (1). Thus, the solution, equation (5), is the same after reproduction ($t > t_r$) as before ($t < t_r$), except that B_c is replaced by $(B_c + \lambda E_c/t_s)$. In subsequent equations, a therefore remains the same before and after t_r , whereas b changes to $b' \equiv (b + \lambda/t_s)$. Consequently, because egg production continues throughout life, the actual asymptotic mass decreases from $M = (ab)^4$ to $M' = (ab')^4 = (1 + \lambda/bt_s)^{-4} M$. As an example, our fit to cod data ($M' \approx 25$ kg) gives $b' \approx 1.3 \times 10^{-3} \text{ days}^{-1}$. To get a rough estimate for the reproductive contribution we take $\lambda \approx 10\%$ (refs 11, 21) and $t_s \approx 100$ days and obtain $\lambda/t_s \approx 1 \times 10^{-3} \text{ days}^{-1}$, giving $b \approx 0.3 \times 10^{-3} \text{ days}^{-1}$. This value indicates that reproduction represents a significant portion of energy allocation. Thus, the proportion of maintenance energy allocated to reproduction relative to other activities, $E_c(dN_c/dt)/N_c B_c \approx \lambda/bt_s$, could be as much as a factor of 3. Consequently $M'/M = (1 + \lambda/bt_s)^{-4}$ could be as small as 10^{-2} . Thus $M \gg m$, so, for times before first reproduction ($t < t_r$), the solution is insensitive to $b = a/M^{1/4}$ and growth is determined primarily by a . In general, separate equations operate before and after t_r ; for most indeterminate growers, however, t_r is much smaller than lifespan, $t_r \ll t_d$, so growth is well approximated by a single equation—equations (4) or (5)—for all t but with b' (and M') replacing b (and M). These equations therefore apply to indeterminate and determinate growers with maintenance including reproduction and M being interpreted as M' in Table 1 and Fig. 2.

We have derived a very general growth equation from first principles on the basis of the conservation of metabolic energy, the allometric scaling of metabolic rate, and the energetic cost of producing and maintaining biomass (cells). The framework differs from recent work that has focused more on trade-offs involving reproduction and mortality^{2-4,22,23}. Our model attributes the slowing of growth as body size increases to limitations on the capacity of networks to supply sufficient resources to support further increase in body mass. Its power is demonstrated by its ability to quantitatively predict growth curves for both determinate and indeterminate growers, oviparous and viviparous species, ectotherms and endotherms, vertebrates and invertebrates (Fig. 2). The model can be extended to plants. Previously²⁴, a simpler version was presented for trees that included only the second term in equation (1). This was adequate largely because the first term only becomes important at large body sizes and only a small proportion of the trees had masses that approached the asymptotic value. Perhaps the most appealing and powerful feature of our model is that the parameters of the growth equation can be derived from fundamental cellular properties and predicted quantitatively from metabolic measurements that are not directly related to growth. □

Received 2 January; accepted 21 August 2001.

1. Brody, S. *Bioenergetics and Growth* (Hafner Press, Darien, Connecticut, 1964).
2. Charnov, E. L. *Life History Invariants: Some Explorations of Symmetry in Evolutionary Ecology* (Oxford Univ. Press, Oxford, 1993).
3. Stearns, S. C. *The Evolution of Life Histories* (Oxford Univ. Press, Oxford, 1992).
4. Reiss, M. J. *The Allometry of Growth and Reproduction* (Cambridge Univ. Press, Cambridge, 1989).
5. Ricker, W. E. Growth rates and models. *Fish Physiol.* **8**, 677–743 (1979).
6. von Bertalanffy, L. Quantitative laws in metabolism and growth. *Q. Rev. Biol.* **32**, 217–231 (1957).
7. West, G. B., Brown, J. H. & Enquist, B. J. A general model for the origin of allometric scaling laws in biology. *Science* **276**, 122–126 (1997).
8. Brown, J. H. & West, G. B. *Scaling in Biology* (Oxford Univ. Press, Oxford, 2000).
9. West, G. B., Brown, J. H. & Enquist, B. J. The fourth dimension of life; fractal geometry and allometric scaling of organisms. *Science* **284**, 1677–1679 (1999).
10. Alberts, M. *Molecular Biology of the Cell* (Garland, New York, 1994).
11. Peters, R. H. *The Ecological Implications of Body Size* (Cambridge Univ. Press, Cambridge, 1983).
12. Calder III, W. A. *Size, Function and Life History* (Harvard Univ. Press, Cambridge, Massachusetts, 1984).

13. Rogers, D. M., Olson, B. L. & Wilmore, J. H. Scaling for the \dot{V}_{O_2} -to-body size relationship among children and adults. *J. Appl. Physiol.* **79**(3), 958–967 (1995).
14. Weathers, W. W. & Siegel, R. B. Body size establishes the scaling of avian postnatal metabolic rate: an interspecific analysis using phylogenetically independent contrasts. *Ibis* **137**, 532–542 (1995).
15. Xiaojun, X. & Ruyong, S. The bioenergetics of the southern catfish (*Silurus meridionalis chen*). I. Resting metabolic rate as a function of body weight and temperature. *Physiol. Zool.* **63**, 1181–1195 (1990).
16. Brett, J. R. The relation of size to rate of oxygen consumption and sustained swimming speed of Sockeye Salmon (*Oncorhynchus nerka*). *J. Fish Res. Bd Can.* **22**, 1491–1501 (1989).
17. Hamburger, K. et al. Size, oxygen consumption and growth in the mussel *Mytilus edulis*. *Mar. Biol.* **75**, 303–306 (1983).
18. Enquist, B. J., Brown, J. H. & West, G. B. Scaling of plant energetics and population density. *Nature* **395**, 163–165 (1998).
19. Cummins, K. W. & Wuycheck, J. C. Caloric equivalents for investigations in ecological energetics. *Mitt. Int. Verein. Theor. Angew. Limnol.* **18**, 1–158 (1971).
20. Kohler, A. C. Variations in the growth of Atlantic Cod (*Gadus morhua* L.). *J. Fish. Res. Bd Can.* **21**(1), 57–100 (1964).
21. Blueweiss, L. et al. Relationships between body size and some life history parameters. *Oecologia* **37**, 257–272 (1978).
22. Kozłowski, J. Optimal allocations of resources explains interspecific life-history patterns in animals with indeterminate growth. *Proc. R. Soc. Lond. B* **263**, 559–566 (1996).
23. Day, T. & Taylor, P. D. von Bertalanffy's growth equation should not be used to model age and size at maturity. *Am. Nat.* **149**, 381–393 (1997).
24. Enquist, B. J., West, G. B., Charnov, E. L. & Brown, J. H. Allometric scaling of production and life-history variation in vascular plants. *Nature* **401**, 907–911 (1999).

Supplementary information is available on Nature's World-Wide Web site (<http://www.nature.com>) or as paper copy from the London editorial office of Nature.

Acknowledgements

We thank E. Charnov for discussing the role of reproduction in our formalism, L. Thomson for supplying data on salmon and P. Taylor for comments. Support from the National Science Foundation and the National Center for Ecological Analysis and Synthesis are gratefully acknowledged. J.H.B. and G.B.W. also acknowledge the support of the Thaw Charitable Trust and a Packard Interdisciplinary Science Grant.

Correspondence and requests for materials should be addressed to G.B.W. (e-mail: gbw@lanl.gov).

.....
Hyperpolarization-activated channels HCN1 and HCN4 mediate responses to sour stimuli

David R. Stevens*, **Reinhard Seifert†**, **Bernd Bufe‡**, **Frank Müller†**, **Elisabeth Kremmer§**, **Renate Gauss†**, **Wolfgang Meyerhof‡**, **U. Benjamin Kaupp†** & **Bernd Lindemann***

* Department of Physiology, Universität des Saarlandes, D-66421 Homburg, Germany

† Institute for Biological Information Processing, Forschungszentrum Jülich, D-52425 Jülich, Germany

‡ Department of Molecular Genetics, Deutsches Institut für Ernährungsforschung, Arthur-Scheunert-Allee 114-116, D-14558 Potsdam-Rehbrücke, Germany

§ Institute for Molecular Immunology, GSF, D-81377 München, Germany

.....
Sour taste is initiated by protons acting at receptor proteins or channels. In vertebrates, transduction of this taste quality involves several parallel pathways¹⁻⁵. Here we examine the effects of sour stimuli on taste cells in slices of vallate papilla from rat. From a subset of cells, we identified a hyperpolarization-activated current that was enhanced by sour stimulation at the taste pore. This current resembled I_h found in neurons and cardio-myocytes^{6,7}, a current carried by members of the family of hyperpolarization-activated and cyclic-nucleotide-gated (HCN) channels⁸⁻¹³. We show by *in situ* hybridization and immunohistochemistry that HCN1 and HCN4 are expressed in a subset of taste cells. By contrast, gustducin, the G-protein involved in bitter and sweet

taste¹⁴, is not expressed in these cells. Lowering extracellular pH causes a dose-dependent flattening of the activation curve of HCN channels and a shift in the voltage of half-maximal activation to more positive voltages. Our results indicate that HCN channels are gated by extracellular protons and may act as receptors for sour taste.

Whole-cell recordings were performed in slices of vallate papilla (Fig. 1a). In 88 out of 497 excitable cells tested (18%), hyperpolarization activated a slowly developing inward current (Fig. 1b), which was blocked by 2 mM extracellular Cs⁺ (*n* = 9) but not intracellular Cs⁺ (*n* = 6). The activation was determined using a dual-pulse protocol (Fig. 1c). The voltage at which activation was half-maximal (*V*_{1/2}) was -105 ± 5 mV (*n* = 12) (Fig. 1d). The time course of activation was voltage dependent and well described by a single time constant, τ , of 478 ± 56 ms at -90 mV (*n* = 4) and 103 ± 14 ms at -130 mV (*n* = 6). The apparent reversal voltage (extrapolated intercept of the instantaneous current-voltage (*I*-*V*) relation before (-60 mV) and after (-100 mV) activation) was *E*_h = -22.5 ± 9 mV (Fig. 1e, f; *n* = 4). These properties are typical of the hyperpolarization-activated current *I*_h (refs 6, 13).

We challenged 277 of 497 cells by micro-jets of sour stimuli at the taste pore (10 mM citric acid at pH 3.0 or 5.0). In 61 of the 277 cells (22%), the sour stimulus induced an inward current and an increase

in conductance (Fig. 1g). Citrate at pH 6.8 had no effect. Thirty-seven out of sixty-one sour-responsive cells (61%; group 1) also exhibited *I*_h. Nine cells that showed no *I*_h before sour stimulation exhibited *I*_h during sour stimulation (9/61, 15%; group 2). The τ of activation of currents from group 2 was 111 ± 20 ms at -130 mV (*n* = 6). Both group 1 and group 2 cells displayed upregulated *I*_h during sour stimulation (the response of a group 1 cell is shown in Fig. 1h).

The apparent reversal voltage of the sour-induced current in *I*_h-positive cells (extrapolated intercept of the instantaneous *I*-*V* relations before and during sour stimulation) was *E*_{sour} = -15.7 ± 10 mV, which is similar to the value of *E*_h (Fig. 1i). The upregulation of *I*_h paralleled the increase in membrane conductance and the generation of inward current (*n* = 10; Fig. 1j). Extracellular Cs⁺ (1 mM) blocked the sour-induced inward current by 52 ± 10% at -70 mV (*n* = 7; Fig. 1k), strengthening the conclusion that *I*_h contributes to the sour-induced inward current. Of 216 cells not responding to the sour stimulus, only 4 (1.9%) had *I*_h. In all, 37 out of 41 cells exhibiting *I*_h (90%, only group 1) or 46 of 50 cells (92%, groups 1 and 2) were sour-responsive. Thus, the correlation is strong between the presence of *I*_h and the response to the sour stimulus.

Consistent with the presence of *I*_h in taste cells, messenger RNA

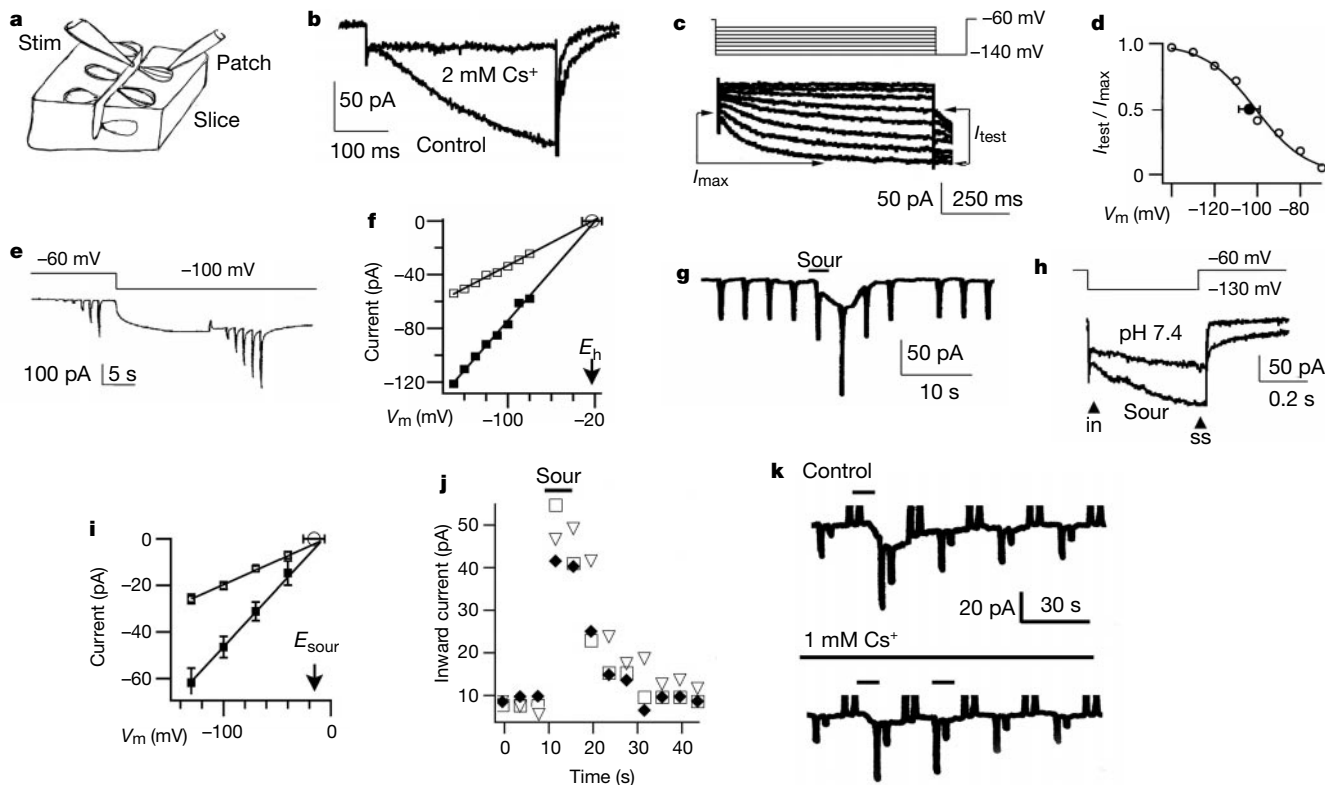


Figure 1 Recordings from rat taste cells. **a**, Slice set-up with micro-jet stimulation (stim) at the taste pore. **b**, Currents activated by stepping from -60 to -130 mV (control), and blockage of this current by 2 mM Cs⁺. **c**, Currents first activated by 870-ms steps from a holding voltage of -60 mV to test voltages from -70 to -140 mV in 10-mV increments. A second step to -140 mV was applied to record tail currents. **d**, Normalized tail currents *I*_{test}/*I*_{max} (see **c** for definition) were plotted against test voltage. A fit with the Boltzmann function $1 - I_{test}/I_{max} = (1 + \exp[N_6(V - V_{1/2})/RT])^{-1}$ yielded an apparent *V*_{1/2} = -105.5 ± 5 mV (*n* = 12) and an apparent *N*₆ = 3.8 ± 0.7 (*n* = 12). As currents did not reach steady state at all voltages, *V*_{1/2} is biased towards negative values. **e**, Currents elicited by 300-ms voltage steps from a holding voltage of either -60 or -100 mV to test voltages ranging from -80 to -150 mV in 10-mV increments. **f**, Instantaneous currents as in **e** plotted against test voltage before (open squares) and after (filled squares) activation

by voltage. The intercept indicates a reversal voltage *E*_h of -22.5 ± 9 mV. **g**, Inward current at -60 mV elicited by application of a sour stimulus (10 mM citrate, pH 5) to the taste pore. Currents elicited by 300-ms steps to -140 mV indicate an increase in conductance of the cell. **h**, Currents activated by a step from -60 to -130 mV at pH 7.4 and pH 5. Instantaneous (in) and steady-state currents (ss) increase during the sour stimulus. **i**, Instantaneous currents from a recording as in **h**, plotted against test voltage before (open squares) and during (filled squares) sour stimulation. The intercept indicates a reversal voltage *E*_{sour} of -15.7 ± 10 mV (*n* = 6). **j**, Time course of holding current at -60 mV (squares), membrane conductance (steps to -130 mV, triangles) and *I*_h (diamonds) during a single sour response. **k**, Inward currents at -70 mV elicited by sour stimuli (horizontal bars) in the absence and presence of 1 mM Cs⁺.

for two of the four known isoforms, HCN1 and HCN4, was detected in rat vallate papilla tissue by polymerase chain reaction with reverse transcription (RT-PCR) (Fig. 2a). The coding region of HCN1 obtained by RACE (rapid amplification of overlapping 5' and 3' complementary DNA fragments) was identical to the published sequence¹⁵. *In situ* hybridization using antisense RNA probes showed the presence of HCN mRNA in a subset of taste cells (Fig. 2b). The HCN mRNAs were of low abundance in vallate papilla tissue, because two consecutive PCRs with nested sets of gene-specific primers were required for their identification, and tyramide amplification was necessary to give clear signals in single cells. In sections of 95 taste buds from the vallate papilla, 481 out of 2,565 cells (19%) were positive for HCN, in good agreement with the electrophysiological data.

Rabbit polyclonal and rat monoclonal antibodies specific for HCN1, -2, -3 or -4 were applied to horizontal sections of rat and mouse vallate papilla. In both rat and mouse, antibodies against HCN1 and HCN4 stained a subset of elongated cells in taste buds (Fig. 3a, b), whereas no staining was observed for HCN2 and HCN3. HCN4-like immunofluorescence was concentrated in the plasma membrane (Fig. 3a, arrow). Co-expression of HCN1 and HCN4 was assessed by applying a rabbit antiserum against HCN4 (green) and a rat monoclonal antibody against HCN1 (red) to the same section (Fig. 3b). HCN1 and HCN4 were colocalized (yellow) in most cells. Few cells stained for only one isoform (Fig. 3b, arrows). The localization of HCN-like immunoreactivity at the basolateral but not the apical membrane is compatible with a model in which protons diffuse through tight junctions to reach the pH-sensitive membrane protein^{16,17}.

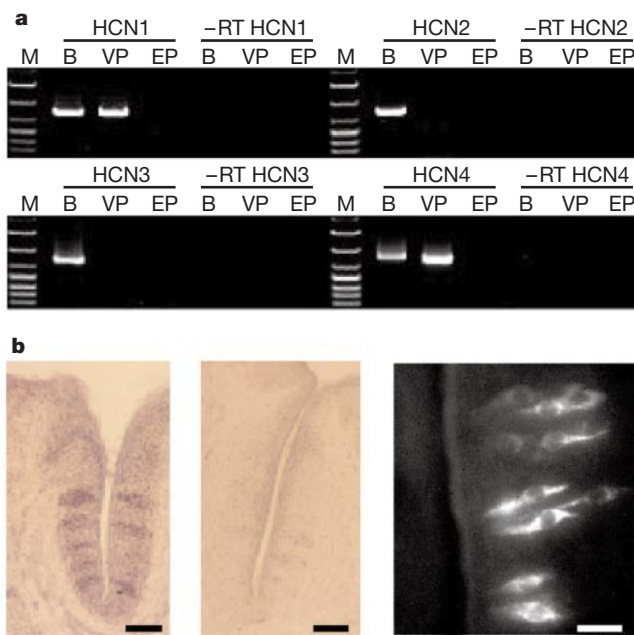


Figure 2 Identification of HCN mRNAs in rat vallate papilla. **a**, Agarose gel electrophoresis of fragments amplified by RT-PCR using subtype-specific primers. mRNAs of HCN1–4 were detected in brain, but only those of HCN1 and HCN4 were found in vallate papilla tissue. The sequence of fragments was identical to the respective sequence of HCN1 and HCN4 from rat brain¹⁵. M, size standard; B, brain (positive control); VP, vallate papilla; EP, non-gustatory tongue epithelium; –RT, no reverse transcriptase present (negative control). Equal amounts of cDNA in the amplification reaction and equal loading of the lanes was verified by RT-PCR of β -actin (not shown). **b**, *In situ* hybridization of rat vallate papilla with HCN RNA probes. Left, hybridized with dioxygenin-labelled antisense RNA; middle, hybridized with sense RNA probes, processed by a standard alkaline phosphatase; right, antisense and tyramide signal amplification. Black bars, 50 μ m; white bar, 20 μ m.

We also labelled sections (Fig. 3c) for both HCN4 (red) and gustducin (green), a G-protein α -subunit that mediates bitter and possibly sweet taste¹⁴. No colocalization was observed, suggesting that sweet- and bitter-responding cells do not express HCN channels. In confocal images taken from eight double-stained sections, we determined the number of HCN-positive cells (70) relative to gustducin-positive cells (94). Given that there are 9.8 gustducin-positive cells per taste bud in the vallate papilla¹⁸, we estimate a value of roughly 7.5 HCN-positive cells per taste bud.

HCN1 and HCN4 currents were studied after heterologous expression of the channels in FLP-IN-293 cells. Figure 4a shows whole-cell HCN1 currents at both pH 7.4 and pH 3.9. The activation threshold at pH 7.4 was near –50 mV and shifted to 0 mV at pH 3.9, showing strong channel activation by protons. Maximal current amplitudes at –120 mV were largely independent of pH. Steady-state inward currents (Fig. 4b) had less rectification at pH 3.9 than at pH 7.4. Figure 4c shows tail currents at –100 mV, from which the voltage dependence of channel activation was determined. In Fig. 4d, mean normalized tail currents are plotted versus membrane voltage V_m for six pH values. Decreasing pH shifted $V_{1/2}$ to less negative voltages and flattened the activation curve. Figure 4e shows the pH dependence of the $V_{1/2}$ and the apparent number of elementary charges (N_e) necessary for activation, as calculated from the Boltzmann equation.

Protons also potentiated HCN4 currents, shifting $V_{1/2}$ and flattening the activation curve (data not shown). However, pH affected the activation kinetics of HCN4 more profoundly than those of HCN1 (Fig. 4f). Decreasing pH from 7.4 to 4.9 led to a strong decrease in the activation time constant τ (Fig. 4g). This acceleration of activation explains the apparent lack of I_h activation in group 2 taste cells at neutral pH. Most likely, these cells express only HCN4 and the voltage pulses used were too short to activate HCN4 appreciably under control conditions (Fig. 4g).

Short pressure applications of sour stimuli to cells expressing HCN1 ($n = 5$; Fig. 4h) and HCN4 ($n = 2$; Fig. 4i) elicited transient

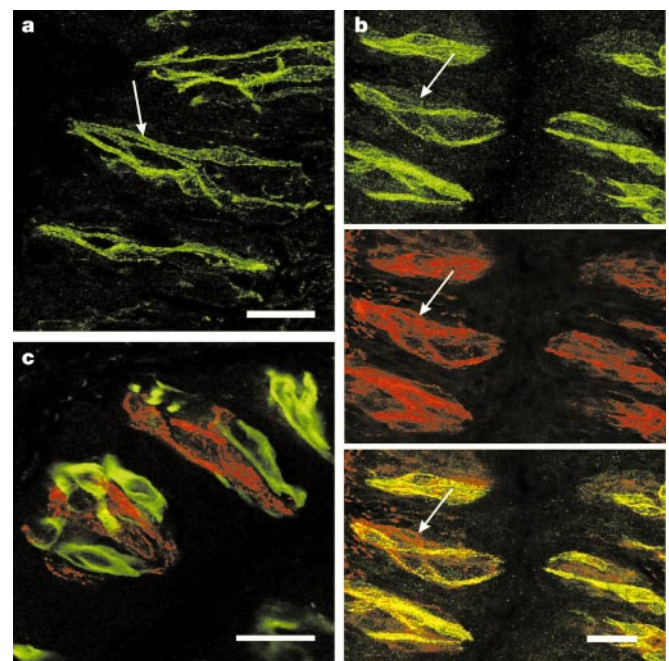


Figure 3 Immunohistochemical localization of HCN1 and HCN4 isoforms. **a**, Horizontal section of mouse vallate papilla, stained for HCN4. Arrow indicates plasma membrane. **b**, In most cases, HCN4 (green) and HCN1 (red) are colocalized; few cells express primarily HCN1 (arrows) or HCN4 (not shown). **c**, Gustducin (green) and HCN4 (red) are expressed in different subsets of cells. Scale bars, 10 μ m.

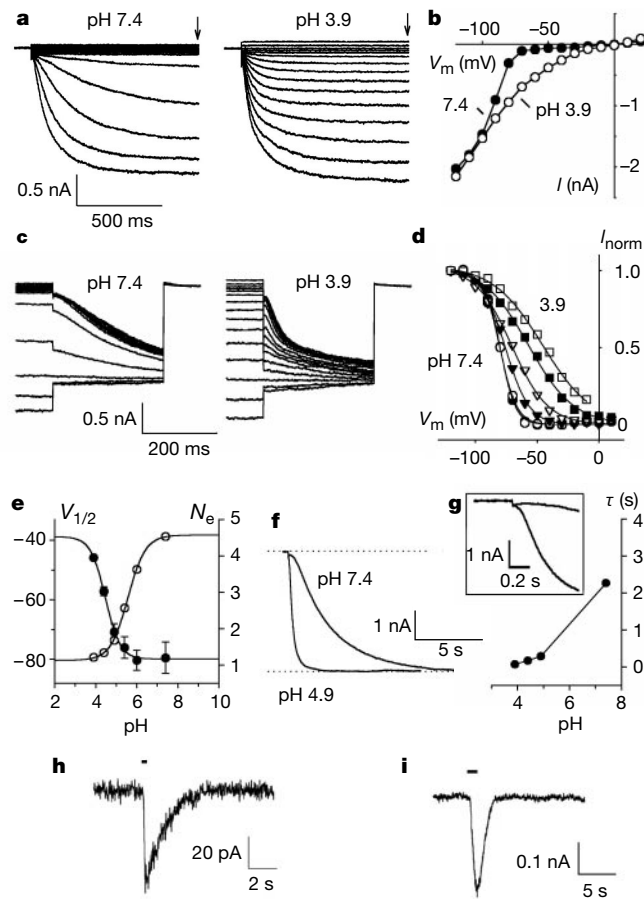


Figure 4 Activation of heterologously expressed HCN1 and HCN4 channels by extracellular protons. **a**, Whole-cell currents of HCN1 channels activated by voltage steps from a holding voltage of 0 mV to various test voltages from +20 to -120 mV in increments of 10 mV at pH 7.4 and at pH 3.9. **b**, Steady-state inward currents of the recordings shown in **a** (arrows), for pH 7.4 (filled circles) and 3.9 (open circles). **c**, Tail currents at -100 mV of the recordings shown in **a**, at pH 7.4 (left) and 3.9 (right). **d**, Voltage dependence of mean normalized tail currents recorded at -100 mV and pH 7.4 (filled circles), 6 (open circles), 5.4 (filled triangles), 4.9 (open triangles), 4.4 (filled squares) and 3.9 (open squares). HCN1 currents were activated for 3 s before tail currents were recorded. Solid lines, Boltzmann functions fitted to data by a least-squares algorithm. Respective values for $V_{1/2}$ and N_e were -79.5 ± 5.3 mV and 4.5 (pH 7.4; $n = 11$); -80.3 ± 3.3 mV and 3.6 (pH 6; $n = 3$); -76.0 ± 3.6 mV and 2.6 (pH 5.4;

$n = 4$); -70.8 ± 2.8 mV and 1.7 (pH 4.9; $n = 6$); -57.1 ± 1.5 mV and 1.3 (pH 4.4; $n = 4$); and -45.8 mV and 1.2 (pH 3.9; $n = 1$). **e**, pH dependence of both $V_{1/2}$ for HCN1 (filled circles) and the number of apparent elementary charges (N_e) necessary to activate HCN1 channels (open circles). **f**, Activation of whole-cell HCN4 currents by a voltage step (14 and 10 s, respectively) from a holding voltage of 0 to -120 mV at pH 7.4 and 4.9. **g**, pH dependence of the activation time constant τ for HCN4. Inset, currents shown in **f** on an expanded timescale. **h**, Rapid response at -50 mV to local application of a sour stimulus in cells expressing HCN1. Bar represents the 0.2-s sour stimulus (pH 4.7) ejected from a patch pipette. **i**, Response at -70 mV to local application to a cell expressing HCN4 channels. Bar represents the 1-s sour stimulus (pH 4.7) ejected from a patch pipette.

inward currents with activation times shorter than 100 ms. The extracellular protons probably interact with a site on the outer surface of the HCN channel, because intracellular acidification causes a negative shift of the activation curve, resulting in inhibition rather than activation of I_h (refs 19, 20).

In conclusion, HCN channels are expressed in a subset of taste receptor cells in the rat vallate papilla. Their currents are activated not only by voltage and cyclic nucleotides, but also strongly and directly by extracellular protons, suggesting that HCN channels function as additional receptors for sour taste. □

Methods

Electrophysiology

The tongue of a juvenile rat (Wistar) was placed for 2 min in ice-cold Tyrode's solution (in mM): 135 NaCl, 5 KCl, 1 CaCl₂, 1 MgCl₂, 10 HEPES, 10 NaHCO₃, 10 D-glucose; pH 7.4. The dissected vallate papilla was sliced in ice-cold Tyrode's solution. The slices (100 μm) were treated with Tyrode's solution containing collagenase (0.05 mg ml⁻¹; Boehringer), Dispase (0.025 mg ml⁻¹; Boehringer) and trypsin inhibitor (0.05 mg ml⁻¹; Sigma) at room temperature for 7 min. In the experimental chamber, slices were superfused with Tyrode's at a rate of 1–2 ml min⁻¹.

We filled heat-polished borosilicate pipettes (3–6 MΩ) with (in mM) 140 KCl, 0.5 CaCl₂, 2.0 MgCl₂, 5 EGTA, 10 HEPES; pH 7.2. After seal formation, access to the cell interior was achieved by stronger suction combined with a large voltage step. To block I_h , 1–2 mM CsCl was added to the Tyrode's solution for at least 10 min.

The sour stimulus comprised 10 mM citric acid, which replaced 10 mM NaCl in the standard Tyrode's solution. The pH was adjusted to 3.0 with HCl and to either 5.0 or 6.8 with NaOH. The stimulus solution was ejected from a patch pipette placed near the taste pore (Fig. 1a), using a Picospritzer (pulse duration 0.1–20 s; General Valve, USA). We could recognize cases in which the stimulus extended too far, and reached the lower dendrite and the soma of the cell, by a reduction in voltage-dependent Na⁺ or K⁺ currents caused by low pH. Repositioning of the stimulus pipette often resulted in recovery of voltage-dependent currents while sour responses were still elicited. This behaviour suggests that sour stimuli are effective when restricted to the apical cellular pole.

Heterologous expression

The cDNAs for human HCN1 and HCN4 (ref. 21) were subcloned into plasmid pCDN5/FRT (Invitrogen). FLP-IN-293 cells (Invitrogen) were transfected with hHCN1 or hHCN4 to generate stable cell lines. Cells were grown and maintained at 37 °C in DMEM cell-culture medium supplemented with 10% fetal calf serum and 1% antibiotic/antimycotic solution (Gibco). Whole-cell recordings were performed in a high K⁺ medium containing (in mM) 150 KCl, 1.8 CaCl₂, 2.8 MgCl₂, 20 'pH buffer'. The solution at pH 7.4 was buffered with HEPES; all other solutions were buffered with MES. pH was adjusted with HCl or N-methyl-D-glucamine-OH (NMDG). The pipette solution contained (in mM) 150 KCl,

1 MgCl₂, 1 EGTA, 10 HEPES; pH 7.4 (NMDG). Time-resolved activation of HCN currents by protons was studied by ejecting a sour stimulus from a patch pipette with a pressure pulse (Eppendorf microinjector 5242). The extracellular and stimulus solutions for these experiments were (in mM) 120 NaCl, 5 NaOH, 20 KCl, 1 MgCl₂, 1 CaCl₂, 10 HEPES; pH 7.4 or 4.7 (HCl). The intracellular solution contained (in mM) 125 KCl, 25 KOH, 10 EGTA, 10 HEPES; pH 7.4.

RT-PCR and *in situ* hybridization

We prepared RNA from isolated vallate papilla tissue²² and synthesized cDNA using standard techniques (RNA-Clean, AGS; Smart cDNA synthesis Kit, Clontech). Aliquots of vallate papilla cDNA, and rat brain cDNA as a control, were amplified by nested PCR using HCN gene-specific primers. HCN1 (GenBank AF247450): forward, 634–656 and 667–694; reverse, 2,000–2,019 and 1,957–1,979. HCN2 (AF247451): forward, 632–655 and 670–693; reverse, 1,991–2,010 and 1,952–1,973. HCN3 (AF247452): forward, 446–466 and 484–505; reverse, 1,796–1,816 and 1,761–1,780. HCN4 (AF247453): forward, 1,181–1,203 and 1,217–1,239; reverse, 2,537–2,559 and 2,503–2,523. Amplification was carried out for 2 min at 94 °C for 35 cycles, including 1 min at 94 °C, 1 min at the respective annealing temperature and 1.5 min at 68 °C using Advantage 2 polymerase (Clontech). The first reaction (4%) was used as template in the second reaction. Annealing temperatures for the first and second reaction were, respectively, 62 °C and 55 °C (HCN1 and HCN2), 66 °C and 70 °C (HCN3), and 66 °C and 65 °C (HCN4).

Vertical cryo-sections (20 μm) of rat tongues were mounted on microscope slides (Merck Eurolab), dried for 30 min at 50 °C, rehydrated for 2 min in PBS (145 mM NaCl, 1.4 mM KH₂PO₄, 8 mM Na₂HPO₄; pH 7.4), and fixed for 10 min in 4% paraformaldehyde/PBS at 4 °C. After washing and prehybridization, sections were hybridized with 200 ng ml⁻¹ dioxigenin-labelled HCN1 RNA (nucleotides 867–1,578; Boehringer) for 16 h at 65 °C in hybridization solution (50% formamide, 0.75 M NaCl, 75 mM sodium citrate, 0.1% bovine serum albumin, 0.1% polyvinylpyrrolidone, 0.1% Ficoll, 250 μg ml⁻¹ yeast transfer RNA, 500 μg ml⁻¹ herring sperm DNA; pH 7.4). Slides were washed once in 5× SSC for 30 min at 65 °C, and twice in 0.2× SSC for 30 min, 65 °C. To block unspecific reactions during the detection, we incubated sections with blocking solution (1% blocking powder (Boehringer) in 0.1 M maleic acid, 0.15 M NaCl). Detection was either by anti-dioxigenin alkaline phosphatase Fab fragments (Boehringer) (1:2,000 in blocking solution, 4 °C, overnight) or by tyramide signal amplification (NEN) and fluorescein-conjugated avidin D (Linaris).

Immunohistochemistry of HCNs

Vallate papillae of rat (Wistar) and mouse (NMRI) were fixed for 15 min by immersion in 4% paraformaldehyde in 0.1 M phosphate buffer at room temperature. Vallate papillae were washed in phosphate buffer, briefly cryo-protected by incubation in 30% sucrose in phosphate buffer and frozen in OCT compound (Sakura). We stained horizontal cryostat sections (20–30 μm) according to standard immunohistochemistry protocols²³. Omission of the primary antibody abolished the staining. In both rat and mouse, staining was obtained with HCN1- and HCN4-specific antibodies, even though the use of rat monoclonal antibodies in sections of rat tongue yielded high background. Images were taken with a laser scanning confocal microscope (Leica TCS). Antibodies were raised against 35-residue peptides that were specific for each of the four HCN isoforms and were tested for specificity by western blotting and immunocytochemistry on rat and mouse retina (F. Müller *et al.*, manuscript in preparation): IHR-7C3 (rat, 1:50) against HCN1; QQA-4A6 (rat, 1:5) against HCN2; TLL-6C5 (rat, 1:5) against HCN3; PpC73K (rabbit, 1:400), SHG-1E5 (rat, 1:5) against HCN4. The gustducin antibody (rabbit, 1:400) was from Santa Cruz Biotechnology. Anti-rabbit Alexa488 and anti-rat Alexa568 secondary antibodies (both goat, 1:500; Molecular Probes) were used.

Data presentation

Throughout the paper, data are presented as means ± s.d.

Received 31 January; accepted 22 August 2001.

1. Gilbertson, T. A., Avenet, P., Kinnamon, S. C. & Roper, S. D. Proton currents through amiloride-sensitive Na channels in hamster taste cells: role in acid transduction. *J. Gen. Physiol.* **100**, 803–824 (1992).
2. Kinnamon, S. C., Dionne, V. E. & Beam, K. G. Apical localization of K channels in taste cells provides the basis for sour taste transduction. *Proc. Natl Acad. Sci. USA* **85**, 7023–7027 (1988).
3. Ugawa, S. *et al.* Receptor that leaves a sour taste in the mouth. *Nature* **395**, 555–556 (1998).
4. Miyamoto, T., Fujiyama, R., Okada, Y. & Sato, T. Sour transduction involves activation of NPPB-sensitive conductance in mouse taste cells. *J. Neurophysiol.* **80**, 1852–1859 (1998).
5. Stewart, R. E., Lyall, V., Feldman, G. M., Heck, G. L. & DeSimone, J. A. Acid-induced responses in hamster chorda tympani and intracellular pH tracking by taste receptor cells. *Am. J. Physiol.* **275**, C227–C238 (1998).
6. Pape, H. C. Queer current and pacemaker: the hyperpolarization-activated cation current in neurons. *Annu. Rev. Physiol.* **58**, 299–327 (1996).
7. Trotier, D. & Doving, K. B. Direct influence of the sodium pump on the membrane potential of vomeronasal chemoreceptor neurones in frog. *J. Physiol. (Lond.)* **490**, 611–621 (1996).
8. Santoro, B. *et al.* Identification of a gene encoding a hyperpolarization-activated pacemaker channel of brain. *Cell* **93**, 717–29 (1998).
9. Gauss, R., Seifert, R. & Kaupp, U. B. Molecular identification of a hyperpolarization-activated channel in sea urchin sperm. *Nature* **393**, 583–587 (1998).
10. Ludwig, A., Zong, X., Jeglitsch, M., Hofmann, F. & Biel, M. A family of hyperpolarization-activated mammalian cation channels. *Nature* **393**, 587–591 (1998).
11. Santoro, B. & Tibbs, G. R. The HCN gene family: molecular basis of the hyperpolarization-activated pacemaker channels. *Ann. N. Y. Acad. Sci.* **868**, 741–764 (1999).

12. Santoro, B. *et al.* Molecular and functional heterogeneity of hyperpolarization-activated pacemaker channels in the mouse CNS. *J. Neurosci.* **20**, 5264–75 (2000).
13. Kaupp, U. B. & Seifert, R. Molecular diversity of pacemaker ion channels. *Annu. Rev. Physiol.* **63**, 235–237 (2001).
14. Wong, G. T., Gannon, K. S. & Margolskee, R. F. Transduction of bitter and sweet taste by gustducin. *Nature* **381**, 796–800 (1996).
15. Monteggia, L. M., Eisch, A. J., Tang, M. D., Kaczmarek, L. K. & Nestler, E. J. Cloning and localization of the hyperpolarization-activated cyclic nucleotide-gated channel family in rat brain. *Brain Res. Mol. Brain Res.* **81**, 129–139 (2000).
16. DeSimone, J. A., Callahan, E. M. & Heck, G. L. Chorda tympani taste response of rat to hydrochloric acid subject to voltage-clamped lingual receptive field. *Am. J. Physiol.* **268**, C1295–C1300 (1995).
17. Pittman, D. W. & Contreras, R. J. Responses of single lingual nerve fibers to thermal and chemical stimulation. *Brain Res.* **790**, 224–235 (1998).
18. Boughter, J. D. Jr, Pumplun, D. W., Yu, C., Christy, R. C. & Smith, D. V. Differential expression of α-gustducin in taste bud populations of the rat and hamster. *J. Neurosci.* **17**, 2852–2858 (1997).
19. Munsch, T. & Pape, H. C. Modulation of the hyperpolarization-activated cation current of rat thalamic relay neurones by intracellular pH. *J. Physiol. (Lond.)* **519**, 493–504 (1999).
20. Zong, X., Stieber, J., Ludwig, A., Hofmann, F. & Biel, M. A single histidine residue determines the pH sensitivity of the pacemaker channel HCN2. *J. Biol. Chem.* **276**, 6313–6319 (2001).
21. Seifert, R. *et al.* Molecular characterization of a slowly gating human hyperpolarization-activated channel predominantly expressed in thalamus, heart, and testis. *Proc. Natl Acad. Sci. USA* **96**, 9391–9396 (1999).
22. Striemi, B. J., Naim, M. & Lindemann, B. Generation of cyclic AMP in taste buds of the rat circumvallate papilla in response to sucrose. *Cell. Physiol. Biochem.* **1**, 46–54 (1991).
23. Müller, F. *et al.* Ligand sensitivity of the α2 subunit from the bovine cone cGMP-gated channel is modulated by protein kinase C but not by calmodulin. *J. Physiol. (Lond.)* **533**, 399–409 (2001).

Acknowledgements

We thank the Deutsche Forschungsgemeinschaft for support.

Correspondence and requests for materials should be addressed to B.L. (e-mail: phblin@uniklinik-saarland.de).

Consequences of a biological invasion reveal the importance of mutualism for plant communities

Caroline E. Christian

Center for Population Biology, One Shields Avenue, University of California, Davis, California 95616, USA

Seed-dispersal mutualisms have a fundamental role in regenerating natural communities^{1,2}. Interest in the importance of seed dispersal to plant communities has been heightened by worldwide declines in animal dispersers^{3–5}. One view, the ‘keystone mutualist hypothesis’, predicts that these human-caused losses will trigger a cascade of linked extinctions throughout the community⁶. Implicitly, this view holds that mutualisms, such as seed dispersal, are crucial ecological interactions that maintain the structure and diversity of natural communities. Although many studies suggest the importance of mutualism^{3,7}, empirical evidence for community-level impacts of mutualists has remained anecdotal^{8,9}, and the central role of mutualism, relative to other species interactions, has long been debated in the theoretical literature^{10,11}. Here I report the community-level consequences of a biological invasion that disrupts important seed-dispersal mutualisms. I show that invasion of South African shrublands by the Argentine ant (*Linepithema humile*) leads to a shift in composition of the plant community, owing to a disproportionate reduction in the densities of large-seeded plants. This study suggests that the preservation of mutualistic interactions may be essential for maintaining natural communities.

Understanding the importance of mutualists to the organization of natural communities is critical for predicting how their decline might alter plant communities. In the fynbos shrublands of South